Ab initio determination of excitation energies and magnetic couplings in correlated quasi-two-dimensional iridates

Vamshi M. Katukuri,[1] Hermann Stoll,[2] Jeroen van den Brink,[1] and Liviu Hozoi[1]

[1]*Institute for Theoretical Solid State Physics, IFW Dresden, Helmholtzstrasse 20, 01069 Dresden, Germany*
[2]*Institute for Theoretical Chemistry, Universität Stuttgart, Pfaffenwaldring 55, 70550 Stuttgart, Germany*

To determine the strength of essential electronic and magnetic interactions in the iridates Sr_2IrO_4 and Ba_2IrO_4—potential platforms for high-temperature superconductivity—we use many-body techniques from wave-function-based electronic-structure theory. Multiplet physics, spin-orbit interactions, and Ir-O hybridization are all treated on equal footing, fully *ab initio*. Our calculations put the lowest d-d excitations of Sr_2IrO_4/Ba_2IrO_4 at 0.69/0.64 eV, substantially lower than in isostructural cuprates. Charge-transfer excitations start at 3.0/1.9 eV and the magnetic nearest-neighbor exchange coupling is 51/58 meV. Available experimental results are fully consistent with these values, which strongly constrains the parametrization of effective iridate Hamiltonians.

PACS number(s): 71.15.Rf, 71.27.+a, 75.30.Et, 75.10.Dg

Whereas the properties of many materials can be understood starting from a theoretical framework in which electrons are weakly interacting, transition metal oxides are a celebrated class of materials for which an independent electron description fails. Prototypical for such strongly correlated electron systems are the $3d$ cuprates, among which are the high-temperature cuprate superconductors. It is well known that electron-electron interactions become progressively weaker when going to heavier transition metal elements, i.e., $4d$ and $5d$ systems, as the spatial extent of d orbitals increases and one might expect a concomitant crossover to a weakly correlated electronic structure. However, the relativistic spin-orbit coupling (SOC) follows the opposite trend—it increases progressively when going to heavier elements. In $5d$ transition metal compounds, e.g., iridates and osmates, the intriguing situation arises where these interactions meet on the same energy scale and SOC can effectively enhance the electronic correlations. This has created a new interest in such correlated compounds since the interplay of crystal field (CF) effects, local multiplet physics, SOC's, and intersite hopping can offer novel types of correlated ground states (GS's) and excitations.[1–14]

The more exotic examples are possible topological states in iridates, such as a topological Mott insulator,[1,2] a Weyl semimetal, and an axion insulator,[3] and the possible realization of the long-sought Kitaev model with bond-dependent spin-spin interactions.[4–6] The 2D square-lattice iridates such as Sr_2IrO_4 and Ba_2IrO_4 are on the other hand appealing because of their perceived structural and magnetic similarity to La_2CuO_4, the mother compound of the cuprate high-T_c (HTC) superconductors, which has promoted them to novel platforms on which HTC superconductivity may be designed.[7–10] To put such considerations on a firm footing it is essential to quantify the different coupling strengths and energy scales, as they for instance appear in effective Hamiltonian descriptions of these correlated systems.[10–13]

Whereas the relevant single-particle hopping integrals can be extracted from tight-binding fits of density-functional-based band structures,[7,11,12,14] for a well-founded evaluation of interactions strengths and excitation energies from first principles one has to rely on wave-function many-body approaches.[15–17] Here, we present the outcome and discuss the implications of *ab initio* many-body calculations for the two so-called 214 iridates, Sr_2IrO_4 and Ba_2IrO_4. We find that for Sr/Ba 214 the lowest d-d excitations of the magnetic GS doublet occur at 0.69/0.64 eV, substantially lower than in isostructural cuprates, where these excitations start at 1.0–1.5 eV.[16] The charge-transfer (CT) continuum of the 2D iridates commences at 3.0/1.9 eV, with the lowest CT excitations confined to the out-of-plane oxygen ligands. It is quite remarkable that in spite of the very different Ir-O-Ir bond angles in the two materials, the strength of the magnetic nearest-neighbor (NN) exchange coupling is rather similar, 51 and 58 meV, respectively. This perhaps unexpected result is a direct consequence of the strong SOC and it sets the 2D iridates apart from the $3d$ transition metal systems, in which superexchange couplings in general depend extremely sensitively on these geometrical factors.

Computational method. For our calculations we rely on multiconfiguration self-consistent-field (MCSCF) and multireference configuration-interaction (MRCI) techniques from modern quantum chemistry.[20] Multiorbital and multiplet physics, SOC's, and O $2p$ to Ir $5d$ CT effects are all treated on equal footing, fully *ab initio*. Since spin-orbit interactions can be switched on and off by hand, we can filter out and explicitly determine the effect of SOC on the electronic structure and excitations. That the quantum-chemical calculations offer insights into the electronic structure of correlated solids that go substantially beyond standard density-functional approaches is well established by now, e.g., for the 2D Cu oxides.[15–17] The magnetic exchange constants[15] and d-d excitations[16] obtained in those systems by quantum-chemical calculations are in excellent agreement with the experiment. Further, spin renormalization effects on the cuprate quasiparticle bands have also been determined.[17] Since the quantum-chemical methodology does not use any *ad hoc* parameters, such calculations are very different from, e.g., hybrid schemes[12,13] based on density-functional theory (DFT) and dynamical mean-field theory (DMFT) and provide information on the electronic structure and excitations that is complementary to for instance a DFT+DMFT approach.[12,13]

In the spirit of modern multiscale electronic-structure approaches, a given region of the extended crystal is treated by advanced quantum-chemical many-body techniques while the
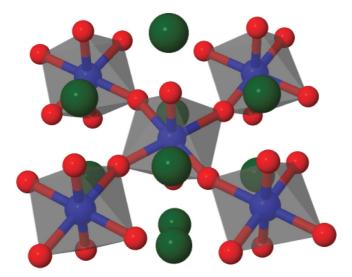
FIG. 1. (Color online) Sketch of the 5-octahedra cluster used for the calculations of crystal-field and CT excitations in Sr_2IrO_4. Ir, O, and Sr ions are shown in blue (dark gray medium), red (gray small), and dark green (dark gray large), respectively. In Ba_2IrO_4, the Ir-O-Ir bonds are straight (Refs. 18 and 19).

remaining part of the solid is modeled at a more elementary level.[15–17] All calculations were performed with the MOLPRO quantum-chemical software.[21] For each of the two compounds, we first designed 5-octahedra clusters (see Fig. 1) to address the nature of the GS electron configuration and of the lowest CF and CT excited states. The ten Sr or Ba ions next to the central IrO_6 octahedron are also included in these clusters. The remaining part of the crystal is modeled as a large array of point charges (PC's) which reproduce the Madelung potential in the cluster region. For the GS calculations, the orbitals within each finite cluster are variationally optimized at the MCSCF level. All Ir t_{2g} functions are included in the active orbital space,[20] i.e., all possible electron occupations are allowed within the t_{2g} set of orbitals. On-site and CT excitations are afterwards computed just for the central IrO_6 octahedron while the occupation of the NN Ir valence shells is held frozen as in the GS configuration. We then analyze the correlated electronic structure of these compounds at the MCSCF and MRCI levels of theory. To partition the O $2p$ valence orbitals into two different groups, i.e., at sites of the central octahedron and at NN octahedra, we use the orbital localization module available with MOLPRO. The implementation of the MRCI and spin-orbit modules are described in Refs. 22 and 23, respectively. To extract the NN superexchange J, we employ PC-embedded 8-octahedra clusters. For those clusters, high-spin and low-spin magnetic configurations are computed for two active Ir sites. To reduce the complexity of the problem and the computational effort, the six adjacent Ir^{4+} ions are modeled as closed-shell Pt^{4+} t_{2g}^6 species.

We used energy-consistent relativistic pseudopotentials for Ir, Sr, and Ba[24,25] and Gaussian-type basis functions from the MOLPRO library. Basis sets of quadruple-zeta quality[20] were applied for the valence shells of the central Ir ion[24] and triple-zeta basis sets for the ligands[26] of the central octahedron and the NN Ir sites.[24] For the central Ir ions we also used two polarization f functions.[24] For farther ligands around the

NN Ir sites we applied minimal atomic-natural-orbital basis sets.[27] All occupied shells of the Sr^{2+} and Ba^{2+} ions were incorporated in the large-core pseudopotentials and each of the Sr $5s$ and Ba $6s$ orbitals was described by a single contracted Gaussian function.[25] To properly describe CT and O $2p$ polarization effects, the ligand bridging the two active Ir sites in the 8-octahedra clusters was described with quintuple-zeta valence basis sets and four polarization d functions.[26]

Splittings of Ir t_{2g} levels. For the (formal) Ir^{4+} t_{2g}^5 valence electron configuration, the strong SOC tends to split off a low-energy $j = 1/2$ doublet. Much attention has been recently paid to obtaining the strength of the SOC λ[7,14,28] and the nature and size of the intersite spin-exchange interactions in a number of different iridates.[4–6,9,29–31] As concerns the magnetic interactions, it has been pointed out that fine details such as the size of the splitting(s) within the valence Ir t_{2g} shell can be extremely relevant. In the layered honeycomb systems, for instance, the trigonal CF splittings appear to strongly influence the nature of the magnetic GS.[30,31]

Whereas the crystal structures of the 214 iridates are similar to that of La_2CuO_4, an important difference between the Sr and Ba 214 systems is that in the former material the IrO_6 octahedra are rotated about the c axis such that the in-plane Ir-O-Ir angles are not $180°$ while in the latter the Ir-O-Ir bonds are straight (see Fig. 1). In both Sr_2IrO_4 and Ba_2IrO_4, the apical Ir-O bonds are longer than the in-plane bonds, 2.06 vs 1.98 Å in Sr_2IrO_4 and 2.15 vs 2.01 Å in Ba_2IrO_4.[18,19] Results for the splittings within the Ir t_{2g} shells in the two materials are listed in Table I. Interestingly, the calculations in which the SOC is switched off show that in the electron representation, the lowest, doubly occupied t_{2g} levels are d_{xz} and d_{yz} in Sr_2IrO_4 and d_{xy} in Ba_2IrO_4. By MRCI calculations, the splittings within the t_{2g} shell are 0.06 and 0.27 eV, respectively (see Table I). We included in the MRCI treatment single and double excitations from the Ir t_{2g} and all O $2p$ orbitals at the central octahedron.

Test calculations in which for the crystal structure of Sr_2IrO_4 we replaced the Sr ions by Ba show that the d_{xz} and d_{yz} levels are still the lowest, as for the set of results listed in the upper part of Table I. Also, if we use the crystal structure of Ba_2IrO_4 but replace Ba by Sr we still find that the lowest-energy t_{2g} level is d_{xy}, as for the results given in the lower part

TABLE I. Splittings within the Ir t_{2g} shells in Sr_2IrO_4 and Ba_2IrO_4, with and without SOC. MCSCF and MRCI results for 5-octahedra embedded clusters, hole representation.

Hole configuration	Relative energies (eV)		
Sr_2IrO_4:			
t_{2g}^1—no SOC, $S = 1/2$	d_{xy}^1	d_{xz}^1	d_{yz}^1
MCSCF	0	0.12	0.12
MRCI	0	0.06	0.06
t_{2g}^1—SOC	$j = 1/2$	$j = 3/2$	
MRCI + SOC	0	0.65–0.81	
Ba_2IrO_4:			
t_{2g}^1—no SOC, $S = 1/2$	d_{xz}^1	d_{yz}^1	d_{xy}^1
MCSCF	0	0	0.19
MRCI	0	0	0.27
t_{2g}^1—SOC	$j = 1/2$	$j = 3/2$	
MRCI + SOC	0	0.69–0.82	

of the table. This shows that our findings of a different energy order of the Ir t_{2g} levels for Sr and Ba 214 in the absence of SOC are strictly related to local Ir-O bonding. Nevertheless, when SOC is accounted for, the splittings between the local doublet $j = 1/2$ and quartet $j = 3/2$ states are about the same in the two compounds. As mentioned above, these calculations were performed on embedded 5-octahedra clusters. In a nonrelativistic picture, the five Ir $S = 1/2$ sites can couple to sextet, quartet, and doublet states. All those different spin configurations entered the spin-orbit calculations so that the energy windows of 0.65–0.81 eV in Sr_2IrO_4 and 0.69–0.82 eV in Ba_2IrO_4 actually include a total number of 64 spin-orbit final states. Also, there are another 31 spin-orbit states in an interval of ≈ 80 meV above the GS, related to the different possibilities of coupling the effective $j = 1/2$ moments of those five Ir sites.

A simplified picture can be obtained by replacing the Ir^{4+} t_{2g}^5 NN's by closed-shell Pt^{4+} t_{2g}^6 ions. The energies of the two components of the $j = 3/2$ quartet, split off by the tetragonal field, are in that case 0.69 and 0.73 in Sr_2IrO_4 and 0.64 and 0.71 in Ba_2IrO_4. These results for the energy separation between the $j = 1/2$ and $j = 3/2$ states imply an effective spin-orbit coupling parameter λ for Sr/Ba 214 of 0.46/0.43 eV, which is surprisingly close to the values of 0.39–0.49 eV extracted for Ir^{4+} impurities from electron spin resonance measurements.[32]

CF and CT excitations. MRCI calculations without SOC put the CF excitations from the t_{2g} to the e_g levels, $t_{2g}^5 \rightarrow t_{2g}^4 e_g^1$ and $t_{2g}^5 \rightarrow t_{2g}^3 e_g^2$, between 2.8 and 6 eV in Sr_2IrO_4 and between 2.0 and 5.0 eV in Ba_2IrO_4. The lowest O $2p$ to Ir $5d$ CT states in MRCI calculations without SOC are at 3.6 eV above the GS in Sr_2IrO_4 and at 1.7 eV with respect to the GS in Ba_2IrO_4. When SOC is switched on, the CF and CT configurations mix and the lowest of those spin-orbit states require excitation energies of 3.0 eV in Sr_2IrO_4 and 1.9 eV in Ba_2IrO_4. For Sr_2IrO_4, those values fit well the resonant inelastic x-ray scattering (RIXS)[33] and optical absorption[34] data, with both types of measurements displaying marked spectral features between 2.5 and 8 eV.

For both Sr and Ba 214, the computed CT gaps are relatively small. Nevertheless, the interaction and mixing of non-CT t_{2g}^5 and CT $t_{2g}^6 \underline{L}$ configurations via SOC is not substantial. It should be noted, however, that a major difference with respect to the 2D $S = 1/2$ cuprates is that in the iridates the lowest CT states have apical hole character, whereas in the 2D Cu oxides the lowest electron-removal states have predominant in-plane O $2p$ character; see, e.g., Ref. 17. The relatively small value we compute for the CT gap in the 214 iridates would put these systems into the charge-transfer category of correlated electron systems.[35]

Magnetic exchange couplings. Our MRCI calculations for the superexchange coupling J include single and double excitations from the Ir t_{2g} and bridging-ligand $2p$ orbitals. Quantum chemical calculations of magnetic couplings in terms of restricted configuration-interaction expansions involving the d orbitals at the active magnetic sites and p functions of the bridging ligand were previously reported, e.g., for La_2CuO_4,[36] providing J's that are in good agreement with the experiment. All possible occupations were allowed within the set of t_{2g} orbitals at the two Ir sites in the present MCSCF calculations, which gives rise to nine singlet and nine triplet

TABLE II. Nearest-neighbor exchange coupling J in Sr_2IrO_4 and Ba_2IrO_4. Negative/positive values denote FM/AF interactions. MCSCF and MRCI results for clusters with two active magnetic centers; see text.

J (meV)	Sr_2IrO_4	Ba_2IrO_4
MCSCF	-19.2	15.4
MCSCF + SOC	28.8	35.7
MRCI + SOC	51.3	58.0

states in the absence of SOC. These MCSCF wave functions were expressed in terms of orbitals optimized for an average of singlet and triplet states. All those eighteen states entered the spin-orbit calculations, both at the MCSCF and MRCI levels. J then corresponds to the difference between the energies of the lowest spin-orbit singlet and triplet states. The three components of the lowest $j_{\text{total}} = 1$ triplet display in both compounds rather small splittings of not more than 3 meV, which shows that the mapping of our *ab initio* results on a symmetric Heisenberg model is controlled. The small effects related to the presence of anisotropic non-Heisenberg terms in the interactions will be the subject of future work.

The resulting J's, as shown in Table II, have a clear physical interpretation. Since the splittings within the t_{2g} shell are relatively small, the three different t_{2g}^5 configurations (see Table I) appear with similar weights in the spin-orbit GS wave functions. Careful analysis of the wave functions for clusters with two active Ir sites however shows that the different order of the t_{2g} levels in Sr and Ba 214 gives rise to subtle differences with respect to the superexchange interactions. For corner-sharing plaquettes or octahedra and t_{2g} active orbitals, the Anderson superexchange implies d-p-d π-type links. For Sr_2IrO_4, when the SOC is switched off, the relevant hole orbital is the in-plane d_{xy} component, as shown in Table I. Due to rotation of the IrO_6 octahedra and bending of the d_{xy}-$p_{x/y}$-d_{xy} bond in Sr 214,[18] the antiferromagnetic (AF) superexchange is not effective and the spin interaction J is actually ferromagnetic (FM); see Table II. With SOC, the t_{2g} hole acquires d_{xz} and d_{yz} character too. Because the $d_{xz/yz}$-p_z-$d_{xz/yz}$ orbital overlap is rather unaffected by bending of the Ir-O-Ir bond, the d-p-d superexchange interactions are much more effective in the presence of SOC. Consequently the magnetic exchange J turns AF, both in MCSCF and MRCI (second column in Table II). Ba_2IrO_4, on the other hand, lacks a bending of the Ir-O-Ir bond.[19] The nature of the hole orbitals in the GS wave function in the absence of SOC therefore matters less in this case: J is large and AF, also in absence of SOC's (third column in Table II). At the MRCI level and including SOC's, J turns out to be somewhat larger in Ba_2IrO_4 as compared to Sr_2IrO_4, 58.0 vs 51.3 meV.

Conclusions. Our detailed investigation of the electronic structure of the 2D $j = 1/2$ Ir oxides Sr_2IrO_4 and Ba_2IrO_4, with *ab initio* many-body quantum-chemical calculations, shows unequivocally that the peak feature observed at about 0.6 eV in the RIXS[9,33] on Sr 214 is directly related to transitions between Ir t_{2g}^5 $j = 1/2$ and $j = 3/2$ states that are in an energy window of 0.65–0.81 eV in Sr 214 and 0.69–0.82 eV in Ba 214. It is interesting to note that the

peak at this energy in optical absorption measurements was assigned to an excitation between Hubbard bands.[34] The experimentally observed "gap" between the 0.6 eV feature and higher excited states that appear above 2 eV in Sr 214[7,33,34] is fully consistent with our calculations. We find that the Sr and Ba 214 compounds differ significantly with respect to their tetragonal CF splittings. While in Sr 214 the lowest t_{2g} states have xz and yz symmetry, in Ba 214 the lowest t_{2g} levels are the xy orbitals. The corresponding tetragonal splittings are 0.06 eV in Sr_2IrO_4 and 0.27 eV in Ba_2IrO_4. The calculations further show that without SOC the distorted Ir-O-Ir bonds in Sr 214 would actually give rise to a FM nearest-neighbor magnetic exchange J. However, the strong SOC reverses the sign of J and causes antiferromagnetism. We find that the dominant magnetic exchange interaction is of Heisenberg type and for Sr 214 has a substantial coupling constant $J = 51$ meV, which compares well with estimates of 45 meV[4] and with RIXS measurements that indicate $J = 60$ meV[9] for this system. For Ba 214, we find a J that is even somewhat larger, which renders it roughly a factor of 2 smaller than the J's in typical 2D cuprates.[15] This might in itself be encouraging for a scenario of magnetic mediated superconductivity in doped 214 iridates. However, the fact the lowest charge-transfer states in 214's have instead of planar, apical oxygen character, points to a destabilization of Zhang-Rice singlets and consequently an effective low energy Hamiltonian that is different from the standard t-J model of doped cuprates.

[1] D. Pesin and L. Balents, Nat. Phys. **6**, 376 (2010).

[2] B.-J. Yang and Y. B. Kim, Phys. Rev. B **82**, 085111 (2010).

[3] X. Wan, A. M. Turner, A. Vishwanath, and S. Y. Savrasov, Phys. Rev. B **83**, 205101 (2011).

[4] G. Jackeli and G. Khaliullin, Phys. Rev. Lett. **102**, 017205 (2009).

[5] J. Chaloupka, G. Jackeli, and G. Khaliullin, Phys. Rev. Lett. **105**, 027204 (2010).

[6] J. Reuther, R. Thomale, and S. Trebst, Phys. Rev. B **84**, 100406 (2011).

[7] B. J. Kim, H. Jin, S. J. Moon, J.-Y. Kim, B.-G. Park, C. S. Leem, J. Yu, T. W. Noh, C. Kim, S.-J. Oh, J.-H. Park, V. Durairaj, G. Cao, and E. Rotenberg, Phys. Rev. Lett. **101**, 076402 (2008).

[8] B. J. Kim, H. Ohsumi, T. Komesu, S. Sakai, T. Morita, H. Takagi, and T. Arima, Science **323**, 1329 (2009).

[9] J. Kim, D. Casa, M. H. Upton, T. Gog, Y.-J. Kim, J. F. Mitchell, M. van Veenendaal, M. Daghofer, J. van den Brink, G. Khaliullin, and B. J. Kim, Phys. Rev. Lett. **108**, 177003 (2012).

[10] F. Wang and T. Senthil, Phys. Rev. Lett. **106**, 136402 (2011).

[11] H. Watanabe, T. Shirakawa, and S. Yunoki, Phys. Rev. Lett. **105**, 216410 (2010).

[12] R. Arita, J. Kuneš, A. V. Kozhevnikov, A. G. Eguiluz, and M. Imada, Phys. Rev. Lett. **108**, 086403 (2012).

[13] C. Martins, M. Aichhorn, L. Vaugier, and S. Biermann, Phys. Rev. Lett. **107**, 266404 (2011).

[14] H. Jin, H. Jeong, T. Ozaki, and J. Yu, Phys. Rev. B **80**, 075112 (2009).

[15] D. Muñoz, F. Illas, and I. de P. R. Moreira, Phys. Rev. Lett. **84**, 1579 (2000).

[16] L. Hozoi, L. Siurakshina, P. Fulde, and J. van den Brink, Sci. Rep. **1**, 65 (2011).

[17] L. Hozoi and P. Fulde, in *Computational Methods for Large Systems: Electronic Structure Approaches for Biotechnology and Nanotechnology*, edited by J. R. Reimers (John Wiley & Sons, Hoboken, 2011), Chap. 6.

[18] M. K. Crawford, M. A. Subramanian, R. L. Harlow, J. A. Fernandez-Baca, Z. R. Wang, and D. C. Johnston, Phys. Rev. B **49**, 9198 (1994).

[19] H. Okabe, M. Isobe, E. Takayama-Muromachi, A. Koda, S. Takeshita, M. Hiraishi, M. Miyazaki, R. Kadono, Y. Miyake, and J. Akimitsu, Phys. Rev. B **83**, 155118 (2011).

[20] T. Helgaker, P. Jørgensen, and J. Olsen, *Molecular Electronic-Structure Theory* (Wiley, Chichester, 2000).

[21] H.-J. Werner, P. J. Knowles, G. Knizia, F. R. Manby, M. Schütz *et al.*, MOLPRO 2010, see [http://www.molpro.net].

[22] A. Berning, M. Schweizer, H.-J. Werner, P. J. Knowles, and P. Palmieri, Mol. Phys. **98**, 1823 (2000).

[23] H.-J. Werner and P. J. Knowles, J. Chem. Phys. **89**, 5803 (1988).

[24] D. Figgen, K. A. Peterson, M. Dolg, and H. Stoll, J. Chem. Phys. **130**, 164108 (2009).

[25] P. Fuentealba, L. von Szentpaly, H. Preuss, and H. Stoll, J. Phys. B **18**, 1287 (1985).

[26] J. T. H. Dunning, J. Chem. Phys. **90**, 1007 (1989).

[27] K. Pierloot, B. Dumez, P. O. Widmark, and B. O. Roos, Theor. Chim. Acta **90**, 87 (1995).

[28] L. J. P. Ament, G. Khaliullin, and J. van den Brink, Phys. Rev. B **84**, 020403 (2011).

[29] I. Kimchi and Y.-Z. You, Phys. Rev. B **84**, 180407 (2011).

[30] S. Bhattacharjee, S. S. Lee, and Y. B. Kim, arXiv:1108.1806.

[31] H. Jin, H. Kim, H. Jeong, C. H. Kim, and J. Yu, arXiv:0907.0743.

[32] B. Andlauer, J. Schneider, and W. Tolksdorf, Phys. Status Solidi B **73**, 533 (1976).

[33] K. Ishii, I. Jarrige, M. Yoshida, K. Ikeuchi, J. Mizuki, K. Ohashi, T. Takayama, J. Matsuno, and H. Takagi, Phys. Rev. B **83**, 115121 (2011).

[34] S. J. Moon, M. W. Kim, K. W. Kim, Y. S. Lee, J.-Y. Kim, J.-H. Park, B. J. Kim, S.-J. Oh, S. Nakatsuji, Y. Maeno, I. Nagai, S. I. Ikeda, G. Cao, and T. W. Noh, Phys. Rev. B **74**, 113104 (2006).

[35] J. Zaanen, G. A. Sawatzky, and J. W. Allen, Phys. Rev. Lett. **55**, 418 (1985).

[36] R. Broer, L. Hozoi, and W. C. Nieuwpoort, Mol. Phys. **101**, 233 (2003).